8. S. Citi and J. Kendrick-Jones, *BioEssays* **7**, 155 (1987).
9. J. S. Sellers, *Curr. Opin. Cell Biol.* **1**, 98 (1991).
10. J. H. Collins, *J. Muscle Res. Cell Motil.* **12**, 3 (1991).
11. S. Lowey, in *Myology*, A. G. Engel and B. Q. Banker, Eds. (McGraw-Hill, New York, 1986), vol. 19, pp. 563–586; P. Vibert and C. Cohen, *J. Muscle Res. Cell Motil.* **9**, 296 (1988).
12. A. Elliott and G. Offer, *J. Mol. Biol.* **123**, 505 (1978).
13. D. A. Winkelmann, H. Mekeel, I. Rayment, *ibid.* **181**, 487 (1985); D. A. Winkelmann, T. S. Baker, I. Rayment, *J. Cell Biol.* **114**, 701 (1991).
14. R. H. Rice and G. E. Means, *J. Biol. Chem.* **246**, 831 (1971).
15. W. R. Rypniewski, H. M. Holden, I. Rayment, *Biochemistry*, in press.
16. L. Silberstein and S. Lowey, *J. Mol. Biol.* **148**, 153 (1981).
17. Y. Nabeshima, Y. Fujii-Kuriyama, M. Muramatsu, K. Ogata, *Nature* **308**, 333 (1984).
18. R. Smith, W. R. Rypniewski, I. Rayment, in preparation.
19. I. Rayment and D. A. Winkelmann, *Proc. Natl. Acad. Sci. U.S.A.* **81**, 4378 (1984).
20. The data to 3.5 Å resolution were recorded at 4°C on a Siemens X1000D area detector; 13 crystals were used to collect the native data. Most of these crystals were translated to expose a new region after 10 to 11 hours in the x-ray beam such that the data were collected from 35 segments. A total of 94,265 reflections were measured, which reduced to 21,370 unique reflections (Theoretical 24,556) with an R_{merge} of 5.3 where
$$R_{merge} = \Sigma\Sigma \{|I_{hi}| - |I_h|\}/\Sigma_{hi} I_{hi} \times 100$$
I_{hi} and I_h are the intensities of the individual and mean structure factors, respectively. These data were recorded with the goal of obtaining a complete, accurate low-resolution x-ray data set that could be used to determine the positions of the heavy atoms in the derivatives. The frame data were processed by the program XDS (*64*) and scaled with the Fox and Holmes algorithm as implemented by P. Evans in the programs Rotavata and Agrovata (*65*). The x-ray data between 3.5 and 2.8 Å were recorded on film at the synchrotron sources located at Cornell (CHESS) and Stanford (SSRL). Data were processed with the software developed by M. Rossmann, modified to operate on a VAX (*66*). The data were merged and scaled with the same software used for the area detector data, except for the inclusion of post-refinement to utilize the partial data (*66*). A total of 178,986 measurements were recorded on 97 films to yield 36,781 independent reflections in the SSRL native data set with an R_{merge} of 9.2. The final native data set consisted of structure factors from 100 to 4.5 Å recorded on the area detector and data from 4.5 to 2.8 Å recorded at SSRL.
21. H. M. Holden and I. Rayment, *Arch. Biochem. Biophys.* **291**, 187 (1991).
22. M. G. Rossmann, *Acta Crystallogr.* **13**, 221 (1960); T. C. Terwilliger and D. Eisenberg, *Acta Crystallogr. Sect. A* **39**, 813 (1983).
23. W. A. Hendrickson and E. E. Lattman, *ibid. Acta Crystallogr. Sect. B* **26**, 136 (1970).
24. B. C. Wang, *Methods Enzymol.* **115**, 90 (1985). The algorithm was written by W. Kabsch (Heidelberg, Germany).
25. M. A. Rould, J. J. Perona, D. Söll, T. A. Steitz, *Science* **246**, 1135 (1989).
26. T. A. Jones, *Methods Enzymol.* **115**, 157 (1985).
27. T. Maita *et al.*, *J. Biochem.* **110**, 75 (1991); G. Matsuda, *Adv. Biophys.* **16**, 185 (1983).
28. The size of the side chains observed in the electron density map was matched to the sequence with the program FITSEQ, available from I. Rayment on request.
29. R. J. Read, *Acta Crystallogr. Sect. A* **42**, 140 (1986).
30. D. E. Tronrud, L. F. Ten Eyck, B. W. Matthew, *ibid.* **43**, 489 (1987).
31. A. T. Brunger, *X-PLOR Manual Version 2.1* (Yale University, New Haven, CT, 1990).
32. L. Szilagyi, M. Balint, F. A. Sreter, J. Gergely, *J. Biochem. Biophys. Res. Commun.* **87**, 936 (1979).
33. D. Mornet, R. Bertrand, P. Pantel, E. Audemard, R. Kassab, *Biochemistry* **20**, 2110 (1981).
34. K. Sutoh, *ibid.* **21**, 4800 (1982).
35. Y. S. Babu *et al.*, *Nature* **315**, 37 (1985).
36. O. Herzberg and M. N. G. James, *ibid.* **313**, 653 (1985).
37. G. Matsuda, Y. Suzuyama, T. Maita, T. Umegane, *FEBS Lett.* **84**, 53 (1977).
38. M. Ikura *et al.*, *Science* **256**, 632 (1992); W. E. Meador, A. R. Means, F. A. Quiocho, *ibid.* **257**, 1251 (1992).
39. Abbreviations for the amino acids residues are A, Ala; C, Cys; D, Asp; E, Glu; F, Phe; G, Gly; H, His; I, Ile; K, Lys; L, Leu; M, Met; N, Asn; P, Pro; Q, Gln; R, Arg; S, Ser; T, Thr; V, Val; W, Trp; and Y, Tyr.
40. C. W. Muller and G. E. Schulz, *J. Mol. Biol.* **224**, 159 (1992); E. F. Pai *et al.*, *EMBO J.* **9**, 2351 (1990).
41. T. D. Pollard, S. K. Doberstein, H. G. Zot, *Annu. Rev. Physiol.* **53**, 653 (1991).
42. A. Musacchio *et al.*, *Nature* **359**, 851 (1992).
43. C. Tesi, T. Barman, F. Travers, *FEBS Lett.* **236**, 256 (1988).
44. R. Mahmood, M. Elzinga, R. G. Yount, *Biochemistry* **28**, 3989 (1989).
45. H. M. Warrick and J. A. Spudich, *Annu. Rev. Cell Biol.* **3**, 379 (1987).
46. I. Rayment *et al.*, *Science* **261**, 58 (1993).
47. K. Yamamoto, *J. Mol. Biol.* **217**, 229 (1991).
48. M. Burke and E. Reisler, *Biochemistry* **16**, 5559 (1977); J. A. Wells and R. G. Yount, *Methods Enzymol.* **85**, 93 (1982).
49. H. White and I. Rayment, *Biochemistry*, in press.
50. J. A. Sleep, K. M. Trybus, K. A. Johnson, E. W. Taylor, *J. Muscle Res. Cell Motil.* **2**, 373 (1981).
51. Y. Okamoto and R. G. Yount, *Proc. Natl. Acad. Sci. U.S.A.* **82**, 1575 (1985).
52. R. G. Yount, C. R. Cremo, J. C. Grammer, B. A. Kerwin, *Philos. Trans. R. Soc. London Ser. B* **336**, 55 (1992).
53. C. R. Cremo, J. C. Grammer, R. G. Yount, *J. Biol. Chem.* **264**, 6608 (1989); J. C. Grammer and R. G. Yount, *Biophys. J.* **59**, 226a (1991).
54. R. S. Goody, W. Hofmann, H. G. Mannherz, *Eur. J. Biochem.* **78**, 317 (1977).
55. E. W. Taylor, *CRC Crit. Rev. Biochem.* **6**, 103 (1979); R. S. Adelstein and E. Eisenberg, *Annu. Rev. Biochem.* **49**, 921 (1980); M. G. Hibberd and D. R. Trentham, *Annu. Rev. Biophys. Biochem.* **15**, 119 (1986); M. A. Geeves, *Biochem. J.* **274**, 1 (1991).
56. R. W. Lymn and E. W. Taylor, *Biochemistry* **10**, 4617 (1971).
57. W. B. Gratzer and S. Lowey, *J. Biol. Chem.* **244**, 22 (1969).
58. E. E. Huston, J. C. Grammer, R. G. Yount, *Biochemistry* **27**, 8945 (1988).
59. K. Wakabayashi *et al.*, *Science* **258**, 443 (1992).
60. Amino acid analyses were performed by L. Mende-Mueller at the Protein and Nucleic Acid Facility, Medical College of Wisconsin, Milwaukee, WI 53226.
61. T. E. Ferrin *et al.*, *J. Mol. Graphics* **6**, 13 (1988).
62. P. J. Kraulis, *J. Appl. Cryst.* **24**, 946 (1991).
63. Y. S. Babu, C. E. Bugg, W. J. Cook, *J. Mol. Biol.* **204**, 191 (1988).
64. W. Kabsch, *J. Appl. Cryst.* **21**, 67 (1988); *ibid.*, p. 916.
65. G. C. Fox and K. C. Holmes, *Acta Crystallogr.* **20**, 886 (1966).
66. M. G. Rossmann, *Methods Enzymol.* **114**, 237 (1985).
67. We thank the co-directors (P. A. Frey, W. W. Cleland, H. Lardy, and G. H. Reed) at the Institute for Enzyme Research for support and discussion, K. Johnson and J. Dewane for technical assistance, and J. Sakon and J. Wedekind for help in the synchrotron data collection and processing. This project was initiated at Brandeis University and continued at the University of Arizona; we thank D. L. D. Caspar, J. H. Law, and M. A. Wells at those institutions for their support and encouragement. Supported by NIH grants (I.R., H.M.H., and D.A.W.). I.R. thanks R. Yount for support and encouragement during the long process of solving this structure.

6 April 1993; accepted 4 June 1993

Structure of the Actin-Myosin Complex and Its Implications for Muscle Contraction

Ivan Rayment,* Hazel M. Holden, Michael Whittaker, Christopher B. Yohn, Michael Lorenz, Kenneth C. Holmes, Ronald A. Milligan

Muscle contraction consists of a cyclical interaction between myosin and actin driven by the concomitant hydrolysis of adenosine triphosphate (ATP). A model for the rigor complex of F actin and the myosin head was obtained by combining the molecular structures of the individual proteins with the low-resolution electron density maps of the complex derived by cryo–electron microscopy and image analysis. The spatial relation between the ATP binding pocket on myosin and the major contact area on actin suggests a working hypothesis for the crossbridge cycle that is consistent with previous independent structural and biochemical studies.

Muscle contraction occurs when two sets of interdigitating filaments, the thin actin filaments and the thick myosin filaments, slide past one another. A widely accepted theory to explain this process is the crossbridge hypothesis of muscle contraction whereby sliding is brought about by crossbridges that extend from the myosin filament and interact cyclically in a rowing motion with the actin filament as adenosine triphosphate (ATP) is hydrolyzed (*1*, *2*).

The myosin head is an actin-activated adenosine triphosphatase (ATPase). Both solution kinetic studies and fiber experi-

ments have demonstrated that transduction of the energy released by ATP hydrolysis into directed mechanical force occurs during product release—adenosine diphosphate (ADP) and inorganic phosphate, P_i—rather than during the hydrolysis step itself (*3*, *4*). The contractile cycle deduced from kinetic studies has shown that Mg^{2+}-ATP rapidly dissociates the actomyosin complex by binding to the ATPase active site of myosin; free myosin then hydrolyzes ATP and forms a stable myosin-products complex; actin recombines with this complex and dissociates the products, thereby forming the original actin-myosin complex. Force is generated during the last step (*4*).

The simple crossbridge cycle has been further elaborated (*5*) to incorporate the observation that release from actin is not obligatory during the hydrolysis of ATP. This requires the introduction of weakly and strongly bound states for the actin-myosin interaction that depend on the nature of the bound nucleotide. Central to this model is the idea that the crossbridge first binds in a weakly binding conformation and then undergoes an isomerization to a strongly binding form. The power stroke must occur within the tightly bound states in order that the energy of hydrolysis can be transduced as movement to the array of filaments (*6*). The process is modulated by the status of the nucleotide binding site, particularly whether or not the γ phosphate is present on the nucleotide.

Initial structural models for the crossbridge portrayed the myosin head as an oar that bound to actin at a point and acted at the same time as both a swivel and a motor (*1*, *7*). The large-scale rotation of the myosin head required by this model has not been substantiated and has led to the proposal (*8*, *9*) that the origin of the rowing-like motion was located at some distance from actin. Subsequent studies demonstrated that the ATP binding site was remote from the actin binding site (*10*, *11*). However, time-resolved fiber diffraction observations indicate that movement of the myosin head is synchronous with the elementary force-generating process in muscle (*12*). Although such studies yielded extensive information about the biochemical properties of the contractile cycle, it proved impossible, without knowledge of the three-dimensional structures of the components and the way in which they interact, to interpret these data in terms of a structural model for muscle contraction. Indeed, until now, there has been no definite information on the way in which chemical energy is transduced into mechanical energy within the bounds of a macromolecular assembly. The structural determinations of actin and the myosin head or subfragment-1 (S1) have changed this situation (*13*, *14*). We now combine these x-ray crystallographic results with information from electron microscopy (EM) to set forth a molecular framework for the contractile cycle. The results suggest the nature of the conformational changes that may occur in the myosin head during force production and indicate which amino acids may be involved in the actomyosin interaction.

Model building. The molecular model of the actomyosin complex was derived from three sources. First, the coordinates of myosin S1 were obtained from the x-ray structure determined at 2.8 Å resolution (*14*). Second, the coordinates for the actin filament (F actin) were derived from the x-ray structure of G actin (*13*, *15*) by fitting and refining a molecular model to the x-ray fiber data from oriented F actin gels (*16*). Finally, the data necessary to combine these high-resolution structures were provided by low-resolution (~30 Å) electron density maps of F actin and S1-decorated F actin which were calculated from images recorded by cryo-EM (*17*, *18*). The model building was performed manually with the program FRODO (*19*). During the first stage, the F actin model was positioned in the F actin EM envelope (Fig. 1). Next, the actin

Fig. 1. Stereo images showing (**A**) the best fit of the atomic model for F actin and the F actin map obtained by cryo-EM and image analysis, and (**B**) good correspondence between the location of Cys^{374} and a gold cluster label (monomaleimide undecagold) which was attached to Cys^{374} and then localized by cryo-EM and difference analysis (*18*). The location of Cys^{374} is indicated by a space-filling model. The atomic model for F actin was obtained by model building and refinement with the use of the atomic coordinates for the actin monomer (*13*) together with low-angle fiber diffraction data (*16*). The EM data for F actin and the Cys^{374} localization were those described in (*18*). The F actin model and the EM map were fit together by changing the phase origin of the EM map until optimal correspondence between the model and map was achieved. The optimal phase origin shift was also applied to the undecagold difference map before display. The final position of the atomic model within the low resolution map was confirmed both by the general correspondence between the gross features of the model and the molecular envelope and by the position of Cys^{374}. Figures 1 and 2 were prepared from a plot file generated from the molecular graphics program FRODO (*19*) and converted to a postscript file with the program FROST (*46*).

I. Rayment and H. M. Holden are in the Department of Biochemistry and Institute for Enzyme Research, 1710 University Avenue, University of Wisconsin, Madison, WI 53705. M. Whittaker, C. B. Yohn, and R. A. Milligan are in the Department of Cell Biology, The Scripps Research Institute, 10666 North Torrey Pines Road, La Jolla, CA 92037. M. Lorenz and K. C. Holmes are in the Department of Biophysics, Max-Planck Institute for Medical Research, Heidelberg, Germany.

*To whom all correspondence should be addressed.

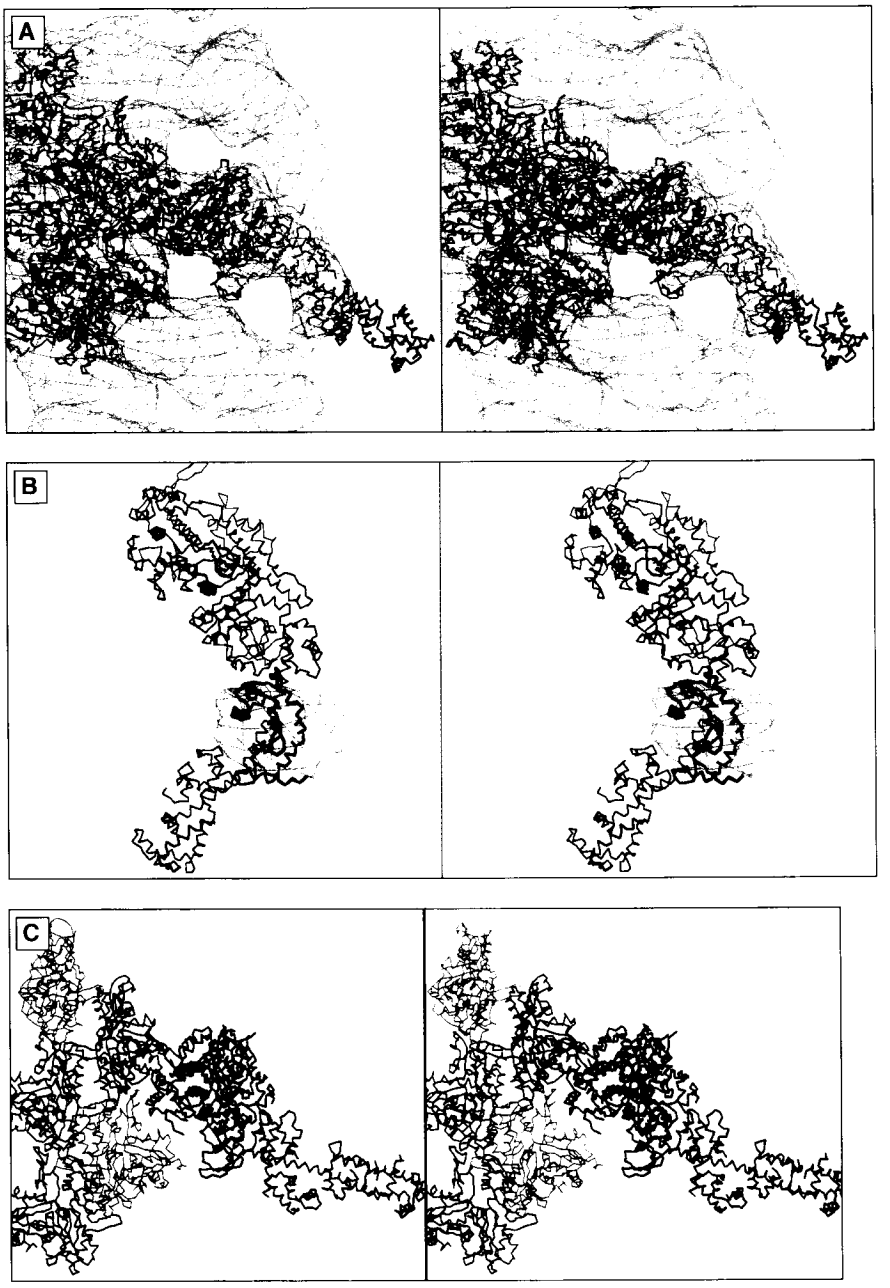

Fig. 2. Stereo images showing (**A**) the best fit of the F actin model and the S1 x-ray structure in the molecular envelope of S1(A2)-decorated F actin obtained by cryo-EM and image analysis (*18*) and (**B**) the good agreement between the location of the essential light chain (A2) and the corresponding difference density. (**C**) An α-carbon plot of five actin monomers and one molecule of S1. Samples for EM were prepared as described (*17, 18*). Cryo-EM and image analyses were carried out as described with some modifications (*17, 18*). Filament stretches of 30 to 32 crossovers were analyzed. As these were generally curved, they were computationally straightened. Prior to processing the helical filaments, density gradients in the images were removed (*17, 18*). The final data set was the average of 20 near and far side data sets from 10 filaments and represents averaging of about 2950 asymmetric units. Data on 22 layer lines extending to a nominal resolution of about ~27 Å were used to calculate the three-dimensional map. No adjustments were made to the data to compensate for the effects of the electron microscope contrast transfer function (ctf). In the data presented, the phases are unaffected by the ctf, however the amplitudes at very low resolution are underemphasized. The F actin and S1(A2)-decorated F actin maps were brought to the same phase origin by a real-space correlation method (*18*). Figures 2C; 3, B and C; and 4, A and B, were prepared with the molecular graphics program MOLSCRIPT (*47*).

envelope was replaced by that of S1-decorated actin, and the S1 x-ray structure was rotated and translated into place (Fig. 2). As the myosin head is highly asymmetric, it was straightforward to position the molecule unambiguously into the envelope. It was immediately clear that the large motor domain of the myosin head (*14*) must be close to actin, whereas the segment that contained the light chain must be at a high radius in the filament (Figs. 2 and 3). The image reconstruction was obtained from chymotryptic myosin S1, which lacks the regulatory light chain so that no density was observed for that part of the myosin molecule. In the fitting process, more emphasis was placed on the structural details at low radius because features at high filament radius in the envelope were underemphasized because of the disorder (*20*). Also, attention was focused on the S1 part of the envelope and no effort was made to minimize or maximize the molecular interactions of the actin and S1 atomic models. Consequently, although the end result gives a good fit between the x-ray structure of the myosin head and the molecular envelope (Figs. 2A and 3A), there is a collision at the site of the actin-S1 interaction involving regions close to the COOH-terminus of actin and the lower 50-kD domain of S1. Although this might appear unacceptable, the x-ray structure of myosin S1 was obtained in a state containing neither bound actin nor nucleotide. Rather than being viewed as a shortcoming of the model, this collision suggests that there may be a conformational change induced in the myosin head when it binds to actin and indeed may contribute to understanding the structural basis of the contractile cycle.

Even though the resolution of the EM is only ~30 Å, the accuracy of the results of the docking procedure is higher because only eight parameters are needed to define the positions of actin and myosin in the image reconstruction. As a consequence it is possible to fit the models for actin and myosin in the reconstruction with an ambiguity of ~5 Å. This magnitude of error does not obviate the conclusions presented in this article. Several independent pieces of evidence support our model. For example, the location of Cys^{374} in the model for F actin is consistent with the electron density associated with a gold cluster label (monomaleimide undecagold) that was bound to this residue (Fig. 1B) (*18*). Likewise the position of the essential light chain is in agreement with the difference electron density (Fig. 1C). The location of the S1-ATP binding site in decorated filaments was previously identified through EM difference mapping by labeling the site with a biotinylated-ATP analog-avidin complex. The ATPase site was 40 to 60 Å away from the actin binding site on the opposite side of the S1 head. The site was ~60 Å from the tip of S1 (*21, 22*). A similar approach was used to locate a reactive cysteinyl resi-

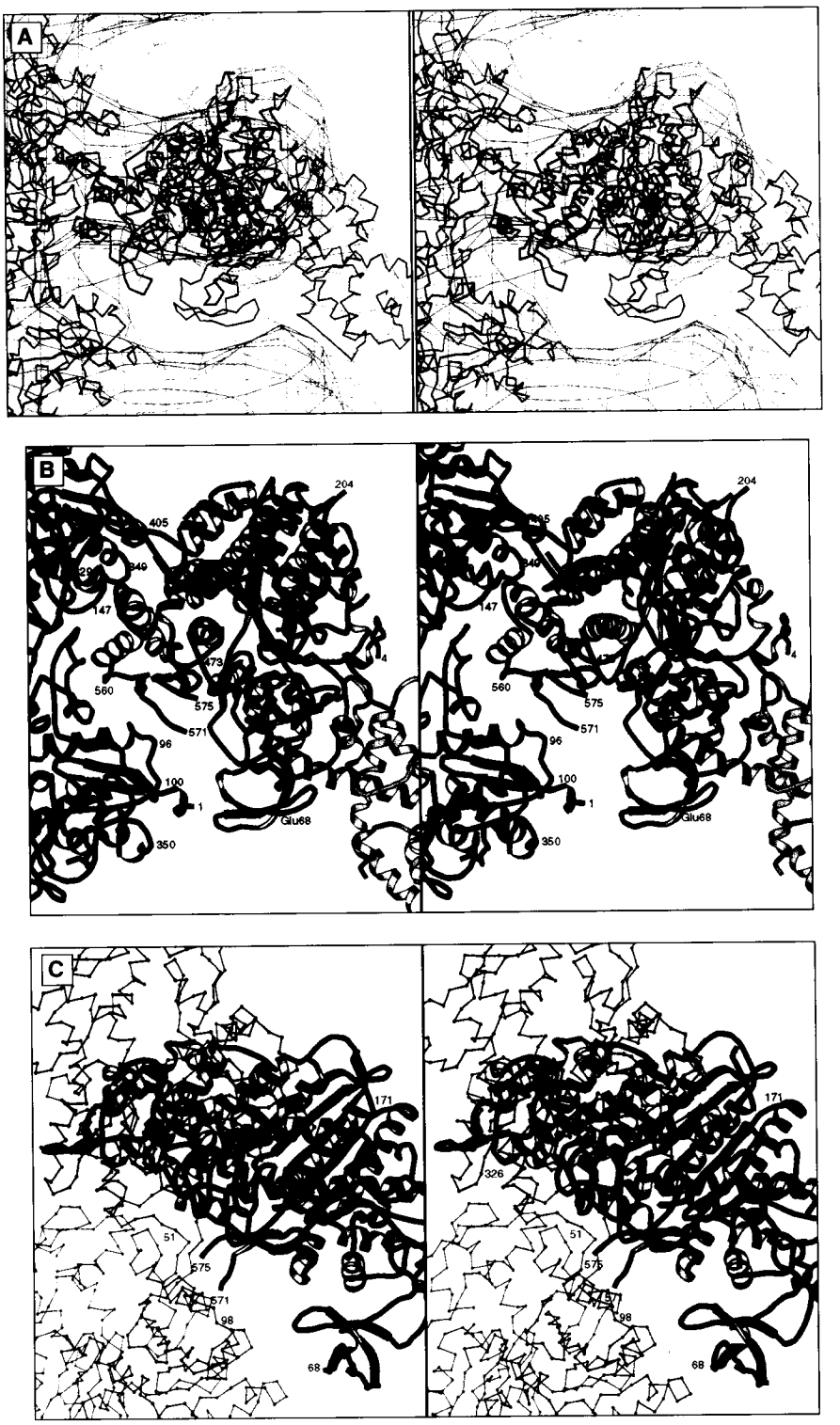

Fig. 3. Enlarged views of the model of the myosin head and its interaction with actin. (**A**) The envelope derived from cryo-EM shows the surface feature identified as the NH_2-terminal domain of skeletal muscle S1 (*20*). Attempts to rotate the head to align the β barrel and the surface feature result in a misfit for the rest of the molecule. In that this barrel projects away from the rest of the molecule it may adopt different positions relative to the head, which may account for the lack of exact correspondence with the EM data. (**B** and **C**) The interaction of myosin with actin viewed from two orientations revealing the details of the actomyosin interface and the relation between the active site and the actin binding site. The secondary structural elements in the myosin heavy chain are color coded according to their position in the primary sequence (*14*). The three tryptic fragments are represented in different colors (*27, 48, 49*). These are the NH_2-terminal 25-kD, the central 50-kD, and one of the COOH-terminal 20-kD fragments, colored in green, red, and blue, respectively. The 50-kD and the 20-kD fragments have been shown to interact with actin (*27, 50*). In (B) the equivalent positions of residues crosslinked in chicken gizzard heavy meromyosin are indicated. In (C) the actomyosin complex has been rotated 90° relative to (B) and shows the position of the nucleotide binding pocket relative to the actin-myosin interface.

due (SH1) on myosin S1 in decorated filaments. It was found that SH1 and the actin binding sites were 50 to 60 Å apart on the same side of the S1 head (*22, 23*). These data are consistent with the model presented below.

The NH_2-terminal region of skeletal myosin (type II) sequences contain a segment that is absent from several non-muscle myosins (type I) (*24*). In the x-ray structure of chicken skeletal myosin S1, this region forms a small antiparallel β barrel (residues 36 to 78) that hangs away from the rest of the head (Figs. 2C and 3). This tertiary structural motif is associated with a protuberance in the image reconstruction of skeletal myosin S1 that is absent from reconstructions of myosin I (*20*). In the model of myosin-decorated F actin, the NH_2-terminal β barrel of one head is in close contact with a second molecule of S1. This is consistent with crosslinking evidence that a specific linkage can be formed between two adjacent heads when they are bound to actin but not when free in solution (*25*). One such point of interaction has been accurately identified for chicken gizzard heavy meromyosin by sequencing the crosslinked peptides (*26*). In this case, the linkage is between Lys^{65} and Glu^{168}, which correspond to Glu^{68} and Glu^{171} in the chicken skeletal muscle sequence. These amino acid residues are 12 Å apart in our model.

Finally, proteolytic studies have shown that the segment between residues Gly^{635} and Lys^{641} in the chicken skeletal heavy chain sequence is protected from hydrolysis when it is bound to actin (*27*). This region is located in the actin myosin interface in our model and thus would be expected to be resistant to proteolysis. Taken together, the above observations place severe constraints on the position of the myosin molecule as it packs around the filament.

General features of the actomyosin model. The bulky motor domain of S1 binds tangentially to the actin filament at an angle of about −45° to the filament axis (Fig. 2C). The thin tail, consisting of the light chain binding region of S1, projects away and tangential to the filament axis at an angle of about 90°. A short helix comprising residues Pro^{830} to Lys^{839} terminates the COOH-terminal part of the S1 heavy chain. In the model, this helix is oriented

at an angle of ~20° with respect to the filament. If the model were placed in the correct location in the sarcomere, the helix would point toward the M line and would represent an appropriate mechanical arrangement for S1 to apply tension to the rod portion of the myosin molecule.

A distinctive feature of the structure of S1 is a narrow cleft that extends from under the nucleotide binding site to the end of the head. This cleft divides the near axial one-third of the head into two domains; the upper and lower domains of the 50-kD segment of the heavy chain (*14*). The cleft, relative to the actin-myosin interface, (Figs. 3 and 4A) lies at an angle of ~30° to the actin filament axis. Opening and closure of this cleft is the most likely mechanism for communication between the nucleotide binding site and the actin binding site as described below. An important feature of the actomyosin interaction is that it involves interactions in the rigor state from both sides of the narrow cleft that splits the 50-kD segment of the myosin head together with the first helix of the 20-kD region. This suggests that formation of the tightly bound state from the weakly bound state is a sequential, multistep process that might first involve formation of a stereospecific interaction between actin and the lower domain of the 50-kD segment followed by cleft closure and incorporation of interactions from the upper domain. Each myosin head interacts with two actin monomers forming primary and secondary binding sites (Fig. 3B). The primary binding site on S1 involves interactions with both subdomains 1 and 3 of one actin molecule and a smaller interaction with the next actin molecule down on the actin helix, whereas the secondary site involves a distinct interaction with the neighboring molecule one turn down. Because of anticipated domain movements in the heavy chain, conformational freedom of the surface loops on both actin and myosin, and possible errors in the modeling process, it would be inappropriate to discuss the exact relation between amino acid residues at the binding sites. However, the general features of the interactions are consistent with kinetic and physical observations on actomyosin as described below.

Examination of the myosin S1 primary binding site suggests that it is potentially composed of three types of interactions with actin: (i) an ionic interaction involving a flexible loop, (ii) a stereospecific interaction involving hydrophobic residues, and (iii) a strengthening of this interaction by the recruitment of additional loops from the upper 50-kD domain. The following discussion is based on the amino acid sequences for rabbit and chicken skeletal muscle actin and myosin, respectively (*28*, *29*).

The docking process places the segment between amino acid residues Tyr^{626} and Gln^{647} of myosin (50- to 20-kD junction) into the actomyosin interface (Fig. 3, A and B). This segment is disordered in the x-ray structure and contains five lysines and nine glycines. These lysine residues are protected from proteolysis in the presence of actin thereby suggesting that they are flexible in solution and either are physically protected by actin (*27*) or only adopt a distinct conformation when bound in the actomyosin interface. From the location of residues Tyr^{626} and Gln^{647}, the intervening 20 residues would be close enough to interact with the six negatively charged residues located between Asp^{1} and Glu^{4} and including Asp^{24} and Asp^{25} on actin. This is consistent with the observation that this segment on myosin can also be chemically crosslinked to the NH_2-terminus of actin (*30*). This interaction is expected to be predominately ionic (five lysines in the loop and six carboxylic acid groups near the NH_2-terminus of actin) and should be sensitive to ionic strength. This component of the structure could be partially responsible for the ionic strength–dependent "weak binding" established as a characteristic of low ionic strength actomyosin interaction (*31*). These interactions might allow the head to adopt a range of orientations while in close proximity to actin. Additional evidence for the involvement of the NH_2-terminal segment of actin in the actomyosin interaction is provided by the observation that when these carboxylic acid containing residues of actin are mutated to histidines, filaments of the mutant actin exhibit ATP-dependent myosin binding but are unable to support movement in an in vitro motility system (*32*).

A potential stereospecific interaction between myosin and actin involves two segments of the S1 heavy chain sequence

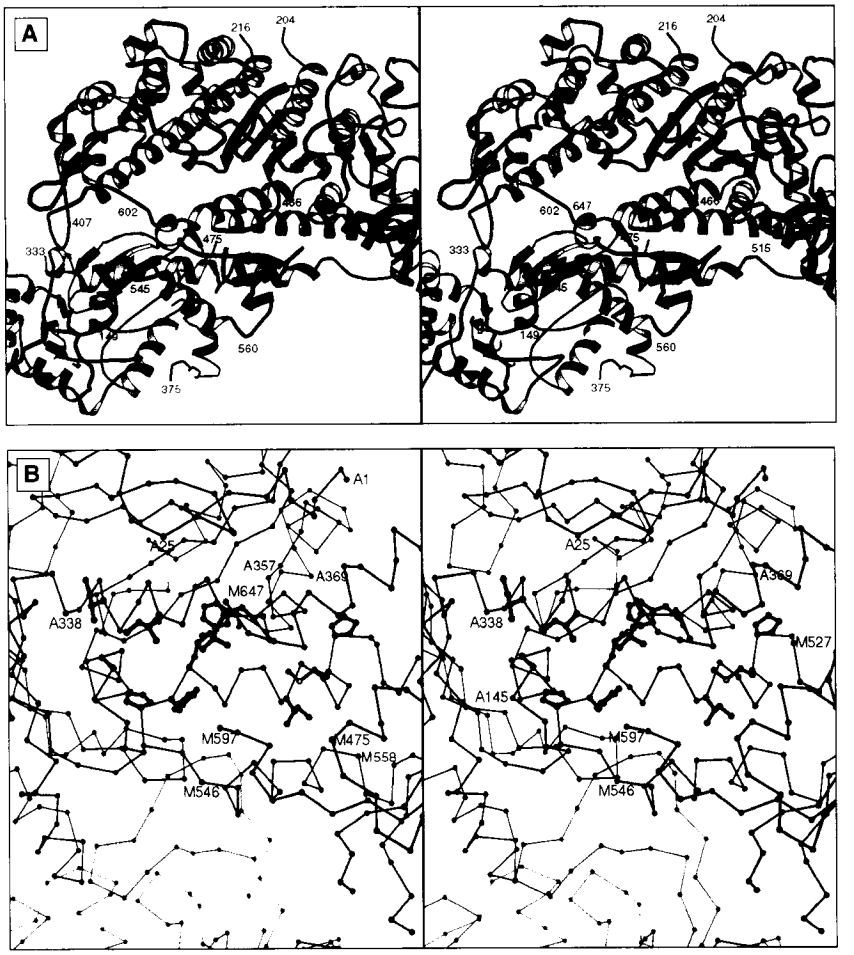

Fig. 4. Close-up views of the actomyosin interface. (**A**) Interaction between actin and myosin viewed along the thin filament axis toward the M line. This stereo reveals the relation between the narrow cleft that divides the 50-kD region of the myosin head and actin. The phosphate binding loop, as indicated by the sulfate ion, lies above the start of the cleft. (**B**) A few of the residues on actin and myosin located in the interface in the current model. Given the expected conformational change in myosin when it binds to actin and the errors in the modeling process, it is inappropriate to consider the exact interaction between the residues. However, it is compelling that this orientation places exposed hydrophobic residues on both actin and myosin in the same interface region.

and two segments of actin (Figs. 3B and 4A). On myosin this occurs through the heavy chain segment from Pro^{529} to Lys^{553}, which consists of a helix that extends from Gly^{516} to Phe^{542}, a loop from Pro^{543} to Thr^{546}, and a second helix from Asp^{547} to His^{558}. The first helix contains a prominent bulge at Pro^{529}. These two helices on myosin run at an angle of ~10° to each other, are located at the end of the lower domain of the 50-kD segment, and are in close proximity to residues Ile^{341} to Gln^{354} and Ala^{144} to Thr^{148} of actin. In addition, residues Asn^{552} to His^{558} of myosin are close enough to make contact with residues His^{40} to Gly^{42} in the actin subunit below. Residues Gln^{647} to Lys^{659} of the myosin heavy chain are also located in the actin-myosin interface. These are the first residues observed after the missing loop at the junction of the 50- and 20-kD segments of the myosin heavy chain.

Two general features of the stereospecific interaction are evident. (i) Exposed hydrophobic residues on the surface of actin (residues: Ala^{144}, Ile^{341}, Ile^{345}, Leu^{349}, and Phe^{352}) and myosin (residues: Pro^{529}, Met^{530}, Ile^{535}, Met^{541}, Phe^{542}, and Pro^{543}) are placed in close proximity. This area also contains potentially complementary ionic and polar groups. (ii) The best fit of the models to the image reconstruction produces a collision between the actin and myosin that could be relieved by moving the entire myosin molecule a few angstroms away from the actin filament or by closure of the narrow cleft that extends from under the nucleotide binding pocket to the actomyosin interface and separates the upper and lower domains of the 50-kD segment. The first possibility seems unlikely because after movement of the S1 molecule, it would no longer be contained within the envelope of the reconstruction. Thus closure of the narrow cleft in myosin on forming the rigor complex is the most likely occurrence and provides a line of communication between the actin binding site and nucleotide binding site.

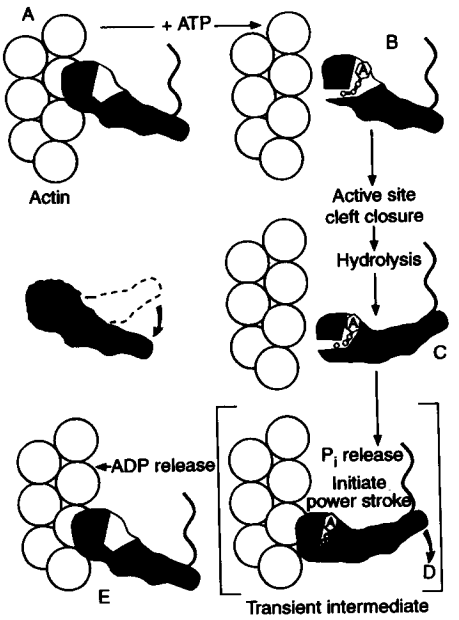

Fig. 5. The contractile cycle incorporating structural features of the myosin head and their proposed involvement in the cycle. Actin is represented as a sphere. In the near axial third of the myosin head, the narrow cleft that splits the 50-kD segment of the myosin heavy chain sequence into two domains is for simplicity represented as a horizontal gap perpendicular to the filament axis. In the model, this cleft lies at an angle of ~30° to the filament axis and the opening and closing of the cleft would not be evident from this view. The representation of the nucleotide-bound state and its associated conformational change relative to the x-ray structure of myosin is conceptual in nature.

In addition to the loop located at the 50- to 20-kD junction there is a second loop, and this one interacts with actin. The segment between Arg^{405} and Lys^{415} on myosin extends toward the actin filament and forms a close contact with residues Pro^{332} to Glu^{334} on actin. In the x-ray structure, this loop is stabilized by an interaction with a symmetry related molecule in the crystalline lattice. It is likely that this loop can adopt a number of conformations. The importance of this segment in normal muscle function has been implicated from genetic studies of familial hypertrophic cardiomyopathy. These investigations have shown that mutation of residue Arg^{403} to Gln in human β cardiac myosin (405 in the chicken sequence) is a factor in this disease (*33*). It is also known from in vitro motility studies that this mutation alters the kinetic properties of myosin S1 even though it is located far from the nucleotide binding site (*34*). In addition, an amino acid sequence comparison reveals that the phosphorylation site, important for regulation of nonmuscle myosins (type I), is close to this loop (*24*). It is compelling that the phosphorylation site is located in the actomyosin interface.

The segment of myosin S1, from residues Lys^{567} to His^{578}, forms an exposed loop that has few contacts with the rest of the molecule and extends toward a second actin monomer below the primary binding site (Fig. 3B). The electron density associated with this segment in the x-ray structure is weak (*14*) suggesting that it is rather flexible. Although this segment is not directly in contact with actin in the model, it could easily extend across the gap and make contact with actin residues Tyr^{91} to Glu^{100}. An important role for this interaction is suggested by studies of mutant actin. When Glu^{99} and Glu^{100} are changed to histidines, filaments of the mutant actin show ATP-dependent myosin binding, but the in vitro motility is reduced by a factor of five (*35*). This interaction could be predominantly ionic in nature since it involves positively charged residues on myosin (Lys^{572} and Lys^{574}) and negatively charged residues on actin. These are conserved residues in vertebrate skeletal myosins. Such an interaction would account for the connection between actin and the myosin head seen in the image reconstructions of decorated actin (*18*). Since, in our model, myosin interacts with two actin subunits, this would also account for the tendency of myosin to catalyze the polymerization of G actin (*36*).

The relation between the nucleotide binding site and the actin binding site on myosin S1 is shown in Fig. 3C. The active site may be identified by the location of a sulfate ion in the phosphate binding loop lying at the bottom of a wide open pocket. It is immediately clear that these critical components of the myosin molecule are separated by at least 35 Å as was predicted (*13, 37*). The nucleotide binding pocket, which is in an open conformation, faces away from the F actin filament and is inclined at an angle of approximately 45° to the filament. It is estimated that closure of this pocket would result in a movement of the COOH-terminus of the heavy chain, relative to actin, by at least 50 Å (*14*).

A model for the molecular basis for muscle contraction. The model of the actomyosin complex is most likely close to that of the rigor state of the actin-myosin complex and offers a view of the molecular arrangement at the end of the contractile cycle. This is only one of the views necessary to fully establish the molecular basis of motility. However, the structure of the myosin head suggests that the power stroke arises from the reversal of domain movements in the myosin heavy chain induced by nucleotide binding and that these occur some distance from the actomyosin interface (*14*). Thus, the single view of the actomyosin complex does provide insights into what may occur during the active parts of the cycle. An immediate suggestion is that myosin forms a tight interaction with actin in only one orientation.

A second implication arises from the observation that the actomyosin interaction comprises a number of distinct components. This implication suggests that binding of myosin to actin during the power stroke is concomitant with a sequential series of interactions beginning with the putative "weak binding" of the myosin loop Tyr^{626} to Gln^{647} and ending with all the described actomyosin interactions in place. A particularly attractive aspect of this idea is that the area of the binding site increases with each step in the sequence, providing a simple

mechanism for generating an increasing binding constant during the process.

Perhaps the most important suggestion arising from the model is that release of the myosin from actin is caused by opening the cleft between the upper and lower domains of the 50-kD heavy chain segment when that part of the nucleotide that carries the γ phosphate binds in the active site pocket. This would serve to disrupt the actin binding site on myosin. The putative γ phosphate binding site lies below the phosphate binding loop (*14*) at the apex of the cleft and provides a way for ATP binding to influence the binding affinity of myosin for actin. These observations, together with the extensive kinetic and structural data available for the contractile system, form the basis for a hypothesis describing the structural basis of the crossbridge cycle (Fig. 5).

Starting at the rigor complex (Fig. 5A), it is assumed that the narrow cleft between the upper and lower domains of the 50-kD segment is in a closed conformation. The binding of nucleotide is seen as a two-step process. In the first stage, only the γ, β, and α phosphates and perhaps part of the ribose moiety of the nucleotide bind to the protein in the P loop at the base of the active site pocket. As a consequence, the narrow cleft between the upper and lower domains of the 50-kD segment opens, thereby disrupting the strong binding interaction between myosin and actin but still allowing the weak binding state (Fig. 5B). This first step is consistent with the reduction of the binding affinity when ATP first binds to myosin. In the second stage of ATP binding, closure of the nucleotide binding pocket around the base (*14*) causes the molecule to undergo a further conformational change leading to a net change in the curvature of the molecule such that the COOH-terminus of the heavy chain would move at least 50 Å relative to the actin binding site. Hydrolysis of the nucleotide follows, giving a metastable state with bound product (Fig. 5C). Implicit in this hypothesis is the concept that the molecule must undergo a conformational change in order to attain a tight complex with the nucleotide and to orient the residues in the active site such that hydrolysis of ATP can occur. In this state, the equilibrium constant for ATP hydrolysis and resynthesis is close to unity at low ionic strength, although it is somewhat higher at physiological ionic strength (*38*). The rate-limiting step in the absence of actin is the release of products from the enzyme. This step is catalyzed by actin.

Rebinding of myosin to actin may consist of a multistep process, involving several conformational states for myosin, in which the first stage is the formation of the weak ionic interaction followed by a stronger but stereospecific interaction with actin involving the lower domain of the 50-kD segment. Incorporation of the components from the upper domain of the 50-kD segment of myosin S1 completes the process and allows the gap between the upper and lower domains to close to produce strong binding. Closure of the cleft is then seen as a way to lower the affinity of the molecule for the γ phosphate, which would then be released. Loss of the γ phosphate would trigger the start of the power stroke and allow the myosin molecule to reverse the conformational change induced by binding of the adenine portion of the nucleotide (Fig. 5D). This would result in a reopening of the active site pocket after which the molecule would return to its rigor state (Fig. 5E). During this process, ADP would be released, and ATP could then rapidly rebind. In the muscle fiber, the myosin head would be tethered to the thick filament through the S2 region of the molecule such that the rate of this conformational change would be determined by the actomyosin lattice movements. One of the implications of this model is that formation of the tight-binding conformation, which serves to initiate the power stroke, will only occur when the myosin head is in a stereospecific orientation with respect to actin filament. This is probably necessary for the efficient transduction of force to thick and thin filament arrays.

The above scheme is consistent with fluorescence and kinetic measurements suggesting that both actin and nucleotide binding to myosin are multistep processes (*5*, *39*, *40*). In addition, the proposed multistage binding of nucleotide agrees with the observation that in the presence of pyrophosphate the binding affinity of myosin for actin is 400 times lower (*41*, *42*) although pyrophosphate is not hydrolyzed and does not support tension development in muscle. In contrast, phosphate alone does not release myosin from actin, which suggests that the conformational change that reduces the binding affinity of myosin for actin requires a minimum of both the γ and β phosphate groups. However, since ADP reduces the binding of myosin for actin by a factor of 40 (*41*), it is likely that the initial binding of ATP to the actomyosin complex includes contributions from the entire nucleotide.

There is considerable chemical evidence for rearrangements in the head associated with the nucleotide binding step as discussed in the description of the x-ray structure (*14*). In addition, chemical crosslinking studies suggest that there are specific conformational changes in the myosin head associated with the 25- and 20-kD segments when it binds to actin (*43*). There have been numerous attempts to observe nucleotide-induced conformational changes in the head. Low-angle neutron scattering measurements do not show any changes of the radius of gyration of myosin S1 when it binds to actin (*44*), whereas low-angle x-ray scattering measurements (*45*) have demonstrated changes associated with nucleotide binding in solution. Both of these observations are consistent with our model since the predicted changes in the structure of the myosin head on binding to actin are small and would be difficult to detect by low-angle scattering.

In this article, we have attempted to correlate the results from the extensive literature on muscle biology and biochemistry with our structure for the actomyosin complex. Many of the properties described here have been foreseen by previous studies based on kinetic, fluorescence energy transfer, antibody labeling and EM measurements (*9*–*11*, *37*). However, the present synthesis offers new insights into the atomic processes of muscle action, and these can be tested by a combination of chemical, biochemical, molecular biological and structural studies.

REFERENCES AND NOTES

1. H. E. Huxley, *Science* **164**, 1356 (1969).
2. A. F. Huxley, *J. Gen. Physiol. (London)* **243**, 1 (1974).
3. R. W. Lymn and E. W. Taylor, *Biochemistry* **10**, 4617 (1971).
4. Y. E. Goldman, *Annu. Rev. Physiol.* **49**, 637 (1987).
5. E. Eisenberg and L. E. Green, *ibid.* **42**, 293 (1980); M. A. Geeves, *Biochem. J.* **274**, 1 (1991).
6. T. L. Hill, *Prog. Biophys. Mol. Biol.* **28**, 267 (1974).
7. A. F. Huxley and R. Simmons, *Nature* **233**, 533 (1971).
8. R. S. Goody and K. C. Holmes, *Biochim. Biophys. Acta* **726**, 13 (1983).
9. R. Cooke, *CRC Crit. Rev. Biochem.* **21**, 53 (1986).
10. K. Sutoh, M. Tokunaga, T. Wakabayashi, *J. Mol. Biol.* **206**, 357 (1989).
11. J. Botts, J. F. Thomason, M. F. Morales, *Proc. Natl. Acad. Sci. U.S.A.* **86**, 2204 (1989).
12. M. Irving, V. Lombardi, G. Piazzesi, M. A. Ferenczi, *Nature* **357**, 156 (1992).
13. W. Kabsch, H.-C. Mannherz, D. Suck, E. Pai, K. C. Holmes, *ibid.* **347**, 37 (1990).
14. I. Rayment *et al.*, *Science* **261**, 50 (1993).
15. K. C. Holmes, D. Popp, W. Gebhard, W. Kabsch, *Nature* **347**, 44 (1990).
16. M. Lorenz and K. C. Holmes, unpublished data.
17. R. A. Milligan and P. F. Flicker, *J. Cell Biol.* **105**, 29 (1987).
18. R. A. Milligan, M. Whittaker, D. Safer, *Nature* **348**, 217 (1990).
19. T. A. Jones, *Methods Enzymol.* **115**, 157 (1985).
20. M. Whittaker and R. A. Milligan, unpublished data.
21. M. Tokunaga, K. Sutoh, C. Toyoshima, T. Wakabayashi, *J. Electron Microsc.* **35** (suppl.), 3107 (1986).
22. T. Wakabayashi *et al.*, *Adv. Exp. Med. Biol.* **226**, 39 (1988).
23. Proceedings of Yamada Conference XI on Energy Transduction in ATPases (Yamada Science Foundation, Osaka, Japan, 1988).
24. T. D. Pollard, S. K. Doberstein, H. G. Zot, *Annu. Rev. Physiol.* **53**, 653 (1991).
25. T.-M. Pepin, D. Mornet, R. Betraud, J.-P. Labbe, R. Kassab, *Biochemistry* **24**, 3024 (1985).
26. H. Onishi, T. Maita, G. Matsuda, K. Fujiwara, *J. Biol. Chem.* **265**, 19362 (1990).
27. D. Mornet, P. Pantel, E. Audemard, R. Kassab, *Biochem. Biophys. Res. Commun.* **89**, 925 (1979);

D. Mornet, R. Bertrand, P. Pantel, E. Audemard, R. Kassab, *Nature* **292**, 801 (1981).
28. J. Vandekerckhove and K. Weber, *Eur. J. Biochem.* **90**, 451 (1978).
29. T. Maita, E. Yajima, S. Nagata, T. Miyanishi, S. Nakayama, G. Matsuda, *J. Biochem. (Japan)* **110**, 75 (1991).
30. K. Sutoh, *Biochemistry* **22**, 1579 (1983); C. Combeau, D. Didry, M.-F. Carlier, *J. Biol. Chem.* **267**, 14038 (1992).
31. B. Brenner, J. Chalovich, L. E. Greene, E. Eisenberg, *Proc. Natl. Acad. Sci. U.S.A.* **79**, 7288 (1982).
32. K. Sutoh, M. Ando, K. Sutoh, Y. Y. Toyoshima, *ibid.* **88**, 7711 (1991).
33. A. A. T. Geisterfer-Lowrance *et al.*, *Cell* **26**, 999 (1990).
34. G. Cuda, L. Fananapazir, W.-S. Zhu, J. R. Sellers, N. D. Epstein, *J. Clin. Invest.* **91**, 2861 (1993).
35. M. Johara *et al.*, *Proc. Natl. Acad. Sci. U.S.A.* **90**, 2127 (1993).
36. L. Miller, M. Phillips, E. Reisler, *J. Biol. Chem.* **263**, 1996 (1988); G. DasGupta, J. White, P. Cheung, E. Reisler, *Biochemistry* **29**, 8503 (1990); T. Chen and E. Reisler, *ibid.* **30**, 4546 (1991); C. Valentinranc, C. Combeau, D. Panteloni, M.-F. Carlier, *J. Biol. Chem.* **266**, 17872 (1991).
37. R. Cooke, *Curr. Opin. Cell Biol.* **2**, 62 (1990).
38. C. R. Bagshaw and D. R. Trentham, *Biochem. J.* **133**, 323 (1973); *ibid.* **141**, 331 (1974); S. S. Rosenfeld and E. W. Taylor, *J. Biol. Chem.* **259**, 11908 (1984).
39. E. W. Taylor, *J. Biol. Chem.* **266**, 294 (1991).
40. C. R. Bagshaw *et al.*, *Biochem. J.* **141**, 351 (1974).
41. L. E. Greene and E. Eisenberg, *J. Biol. Chem.* **255**, 543 (1980).
42. B. Brenner, L. C. Yu, L. E. Greene, E. Eisenberg, M. Schoenberg, *Biophys. J.* **50**, 1101 (1986).
43. R. Betrand, J. Derancourt, R. Kassab, *Biochemistry* **31**, 12219 (1992).
44. P. M. Curmi, D. B. Stone, D. K. Schneider, J. A. Spudich. R. A. Mendelson, *J. Mol. Biol.* **203**, 781 (1988).
45. K. Wakabayashi *et al.*, *Science* **258**, 443 (1992).
46. The program FROST was written by G. Wesenberg, University of Wisconsin; it is available on request.
47. P. J. Kraulis, *J. Appl. Crystallogr.* **24**, 946 (1991).
48. M. Balint *et al.*, *Arch. Biochem. Biophys.* **190**, 793 (1978).
49. L. Szilagyi, M. Balint, F. A. Sreter, J. Gergley, *Biochem. Biophys. Res. Commun.* **87**, 936 (1979).
50. K. Sutoh, *Biochemistry* **21**, 4800 (1982).
51. This work could not have been done without the extensive literature on muscle biology and biochemistry. We thank H. White (E. Virginia Medical School), R. Moss (University of Wisconsin), and Y. Goldman (University of Pennsylvania) for helpful discussions; B. L. Jacobson (University of Wisconsin) for preparation of Fig. 5; and G. Wesenberg (University of Wisconsin) and B. Carragher (University of Illinois) for computational assistance. Supported by NIH grants (I.R., H.M.H., and R.A.M.); an NSF predoctoral felllowship (C.B.Y.); and Established Investigatorships of the American Heart Association (H.M.H. and R.A.M.).

6 April 1993; accepted 1 June 1993